Low-temperature Synthesis and Magnetostructural Transition in Antiferromagnetic, Refractory Nanoparticles: Chromium Nitride, CrN

Anne-Marie Zieschang,[1] Joshua D. Bocarsly,[2] Michael Dürrschnabel,[3] Hans-Joachim Kleebe,[3] Ram Seshadri,*[,2] Barbara Albert*[,1]

[1] Eduard-Zintl-Institute of Inorganic and Physical Chemistry, Technische Universität Darmstadt, Alarich-Weiss-Str. 12, 64287 Darmstadt, Germany

[2] Department of Chemistry & Biochemistry, Materials Department, and Materials Research Laboratory, University of California, Santa Barbara, Santa Barbara California 93106, United States

[3] Department of Materials and Earth Sciences, Electron Microscopy Center Darmstadt (EMC-DA), Technische Universität Darmstadt, Alarich-Weiss-Str. 2, 64287 Darmstadt, Germany

ABSTRACT: Nanostructured chromium nitride (CrN), both a hard material and a high-melting compound that is used in the medical industry and for new energy-harvesting applications, was synthesized phase-pure for the first time via low-temperature solution synthesis in liquid ammonia. TEM analysis confirms the nanoscale character of CrN. The antiferromagnetic properties of the agglomerates of nanoparticles are discussed in comparison to literature data on the bulk materials. SQUID and DSC measurements show the transition from paramagnetic to antiferromagnetic at 258.5 K. *In-situ* low-temperature X-ray diffraction patterns confirm the magnetostructural phase transition at this temperature, not seen before for nanoscale CrN. This structural distortion was calculated earlier to be driven by magnetic stress. The bottom-up synthesis of CrN allows for the production of nearly oxygen- and carbon-free and highly dispersed fine particles.

Introduction

CrN is a high-temperature resistant refractory that is used to enhance the electrical conductivity of ceramics and to design novel tools for medical applications.[1,2] Also, this hard and high-melting substance was discussed recently as a new energy-harvesting material[3] and finds application in form of coatings for corrosion resistance and mechanical hardening of surfaces. It has also been investigated as a potential catalyst[4,5] and high-temperature thermoelectric material[6]. The densification of such compounds is desirable for many purposes but very difficult to achieve for bulk materials obtained by conventional high-temperature synthesis, due to their refractory character. For nanoscale powders of TiN and $Cr_{1-x}Ti_xN$, Wang et al.[7] and Jin et al.[8] observed an improved sintering behavior, respectively, but it has also been shown that samples consisting of powders that are very finely dispersed often contain impurities such as oxygen or carbon. These may negatively impact the densification and the mechanical and functional properties of the final product. Thus, it is of high importance to find new synthesis procedures for small particles of refractory materials like CrN.

Earlier, based on theoretical calculations chromium nitride was presented as a case study for a material that exhibits a structural transition driven by magnetic stress. The rocksalt–*Pnma* transition was understood to be caused by stress anisotropy,[9] while a sudden change in the calculated bulk moduli was discussed controversially.[10,11] The dependence of magnetism of size and crystallinity in nanoscale powders of refractory materials has been in our focus for many years,[12] and thus we will now present our experimental approach to investigate the long-standing phenomenon of the magnetostructural distortion in CrN.

Transition metal nitride nanoparticles are usually produced by solid-gas reactions of the metal, metal chloride or a metal oxide precursor with ammonia (and hydrogen)[8,13-15] or the reaction of the metal chloride with sodium azide.[16] Small scale reactions (e.g. plasma processes)[17,18] or autoclave reactions[19] have been described as well. Pure CrN nanoparticles from solution were not known before, but a sol-gel synthesis procedure was described that resulted in particles with a 2 nm – 4 nm thick carbon coating.[20] In principle, solution synthesis allows for better control over the shape and size of the particles and may reduce the risk of carbon or oxygen incorporation, depending on the solvent and reactants used. Synthesis in liquid ammonia was shown to provide a pathway to oxygen- and carbon-free transition metal nitrides.[21-24] While alkaline and alkaline earth metals in liquid ammonia have been used for the reduction of metal salts for many years,[25-28] chromium salts in liquid ammonia have not been studied extensively yet. To our knowledge, the reaction of chromium salts with an alkaline metal solution to obtain chromium nitride is described here for the first time, although Schmitz-Dumont et al.[29] studied the reaction of hexammine chromium(III) nitrate with potassium amide to produce chromium(III) amide as early as 1941.

CrN as a bulk material has been shown to exhibit a magnetostructural phase transition at T_N = 286 K. When the crystal magnetically orders at this temperature, there is a spontaneous change in crystal

symmetry from a paramagnetic cubic crystal structure (*Fm*-3*m*) to an antiferromagnetic orthorhombic crystal structure (*Pnma*).[10] This transition has been extensively studied as the prototype for strong magnetostructural coupling.[9,30-37] The magnetic properties of nanoscale CrN have not been described before. Here, we use magnetic measurements and *in-situ* X-ray diffraction on nanoparticles of CrN synthesized from $CrCl_3$ and sodium in liquid ammonia to show that pure CrN nanoparticles as small as 10 nm in diameter exhibit the coupled magnetostructural transition. This illustrates the robustness of the strong magneto-structural coupling in this system.

Experimental Section

Synthesis

All glassware was heated *in vacuo* and then flushed with argon three times to remove all traces of water and oxygen. Prior to the synthesis, ammonia (Air Liquide, UHP, < 5 ppm H_2O) was condensed and dried with sodium for 24 h. $CrCl_3$ (Fluka, > 98 %) was used without further purification.

The CrN nanoparticles were produced in a three-neck flask by adding 3.9 equivalents of sodium to a suspension of $CrCl_3$ in about 50 ml of liquid ammonia. The reaction temperature was kept at −78 °C for 1.5 h. During that time, the flask was taken out of the cold bath to be stirred for one minute every 20 minutes. After the reaction, the mixture was allowed to warm to room temperature. When all ammonia had evaporated, the powders were dried *in vacuo* for eight hours, annealed at different temperatures (temperature program in Supporting Information), and then washed with methanol. About 2 g of product can be obtained in one synthesis run. The sample preparation and all of the characterization was carried out without ever exposing the samples to air.

Structural characterization. Low-temperature and room temperature X-ray powder diffraction data was collected by a powder diffractometer (STOE Stadi P, position-sensitive detector) with $MoK_{\alpha 1}$ radiation (Ge(111) monochromator, λ = 0.70930 Å, glass capillary, Debye-Scherrer geometry). Short scans (1 range) from 10-50°, with a step size of 0.5° and 40 s/step were performed for all temperatures. At room temperature an additional long scan (8 ranges) from 5 to 50°, with a step size of 0.5° and 60 s/step was performed. To extract structural parameters from the XRD data, the patterns were refined using the Rietveld method in TOPAS Academic.[38] Bragg peaks were modeled as Pseudo-Voigt peaks with axial divergence asymmetry. An additional refinement of the long scan of the room temperature data was performed using the fundamental parameters peak shape approach to extract particle size information.[38]

Magnetic measurements. Magnetic measurements were carried out in a Quantum Design SQUID magnetometer (MPMSXL). About 25 mg of nanoparticles were loaded into a dry cellulose capsule in a N_2 glovebox. The capsule was then sealed with polyamide tape and placed quickly into the helium environment of the magnetometer. Magnetization was collected as a function of temperature at a fixed magnetic field of 200 Oe.

Differential scanning calorimetry. Differential scanning calorimetry (DSC) measurements were performed using a TA Q2000 calorimeter. A ~7 mg sample of nanoparticles was hermetically sealed inside airtight TZero aluminum pans in a N_2 environment glovebox. Thermograms were recorded upon cooling and heating with a 10 K/min rate over a temperature range of 175 K to 295 K.

Transmission electron microscopy. A 200 kV JEOL JEM 2100F (scanning) transmission electron microscope (STEM) equipped with an Oxford X-Max80 detector was used to determine the microstructure and chemistry on the nanometer scale. Quantitative energy-dispersive X-ray spectroscopy (EDX) analysis was carried out using the Cliff-Lorimer k-factor method. A Gatan transfer specimen holder model 648 was used to protect the samples from oxidation. The evaluation of diffraction data was carried out using the DiffTools script.[39]

Results and discussion

Upon combining the $CrCl_3$ and sodium in liquid ammonia, gas evolution was observed, which could be due to the formation of hydrogen or the vaporization of ammonia. After evaporation of the ammonia, a black solid was obtained. This solid was found to be amorphous by X-ray diffraction, which only showed reflections corresponding to a sodium chloride by-product. After annealing and washing the sample, crystalline CrN nanoparticles were obtained.

Using X-ray powder and electron diffraction, the annealed nanoparticles of CrN were found to be nanocrystalline and single-phase (sodium chloride-type structure, s.g. *Fm*-3*m*). While other authors observed Cr_2N as a side phase when synthesizing CrN through conventional high-temperature routes,[8] we did not observe any reflections of secondary products even after annealing at temperatures as high as 873 K. (Figure 2 (a)).

The TEM investigation confirms the results of the X-ray diffraction. Figure 1 shows conventional diffraction contrast images of a representative CrN agglomerate after annealing at 773 K. From both the bright-field and the dark-field images (Figure 1 (a) and (b)) the particle size can be determined representatively. The mean diameter of the CrN particles that were annealed at 773 K was determined to be 9.8 (± 5.7) nm (303 particles, see Supporting Information). This is in good accordance with the crystallite size determined by Scherrer equation (9.9(1) nm).[38] The diffraction pattern shown in Figure 1 (c) shows polycrystalline diffraction rings. These rings can be indexed using the CrN structure.[40] No extra rings belonging to e.g. Cr_2N were observed. This is in good agreement with the XRD measurements shown in Figure 2 (a). Finally, a high-resolution phase contrast image of single CrN nanoparticles lying on the carbon film is presented in Figure 1 (d). One particle that is oriented along the [001] zone-axis is presented enlarged in the inset to demonstrate that single, crystalline nanoparticles were obtained by this bottom-up process. Furthermore, a phase contrast simulation (using the CrN structure[40] and assuming a Scherzer focus condition and a sample thickness of 4.5 nm) is shown for easier image interpretation. The bright spots correspond to the atomic columns. Energy-dispersive X-ray spectroscopy shows an average nitrogen content of 52.15 ± 1.54 at% and an average chromium content

of 47.85 ± 1.54 at%, indicating a composition of $CrN_{1.09(5)}$ (details in Supporting Information). The chromium to nitrogen ratio was confirmed by elemental analysis, which gave a composition of $CrN_{1.06(3)}$ (details also in Supporting Information). The elemental analysis also shows very small amounts of carbon, hydrogen and oxygen, which are most likely caused by residual methanol on the nanoparticle surface.

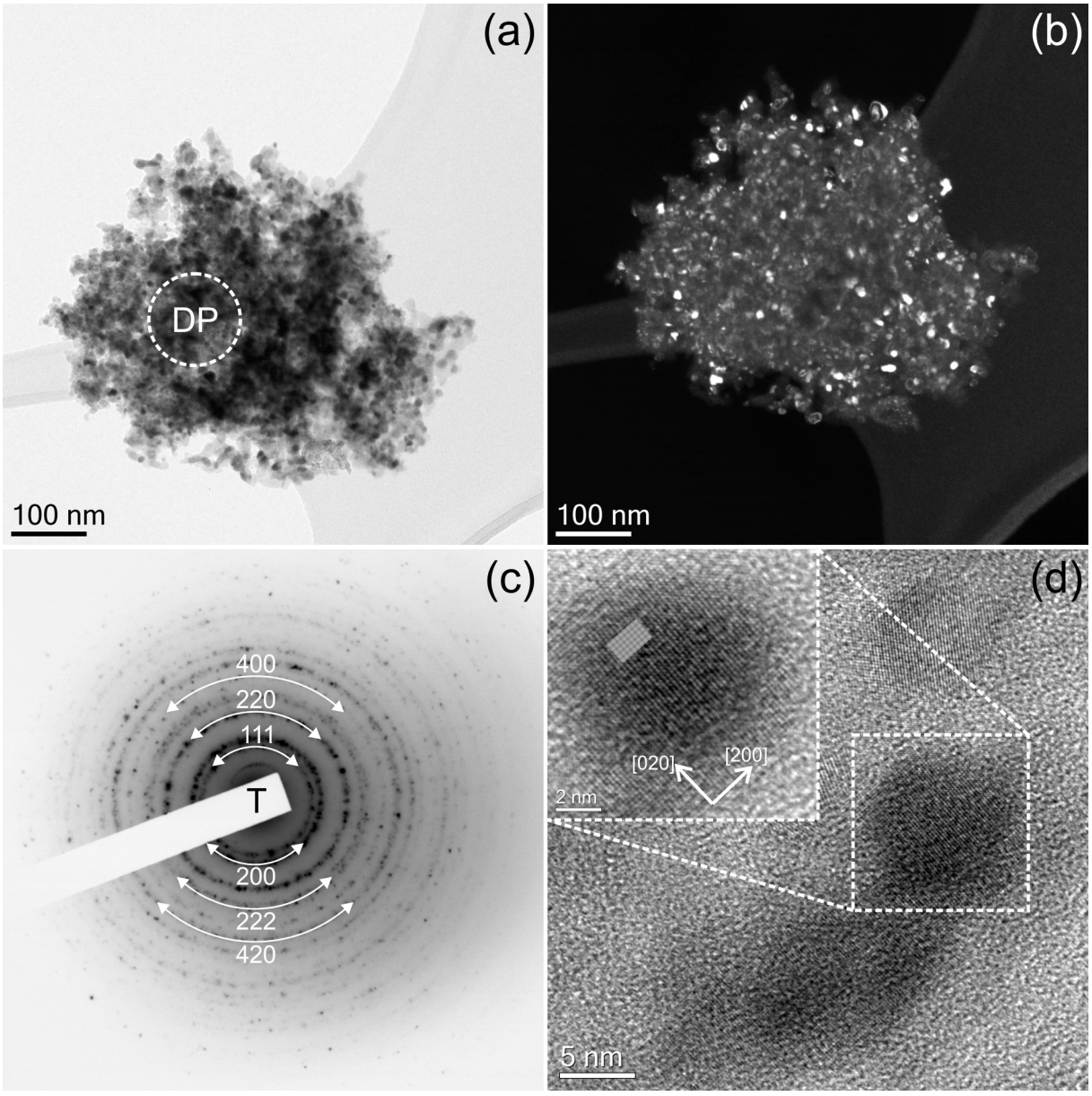

Figure 1: Diffraction contrast images of a representative CrN agglomerate after annealing at 773 K: (a) bright-field and (b) dark-field. (c) Selected area diffraction pattern indexed according to the CrN structure.[40] (d) High-resolution phase contrast images of single chromium nitride particles lying on the carbon film. The inset shows an enlargement of a single spherical CrN nanoparticle oriented in [001] zone axis orientation.

CrN nanoparticles (annealed at 873 K) were investigated by *in-situ* low temperature X-ray powder diffraction for the first time. When annealed at 873 K instead of 773 K, the crystallites grew from 9.9(1) nm to 13.2(1) nm as determined by Scherrer equation. Low-temperature *in-situ* X-ray powder diffraction was performed on both samples. Both samples show a structural transition from the rock salt structure at high temperature to orthorhombic at low temperature, however, this phase transition can be seen more clearly in the sample annealed at 873 K as the peaks are sharper. Figure 2 shows diffraction patterns of CrN nanoparticles after annealing at 873 K collected at 298 K and 193 K. The data was refined using the Rietveld method using the structure of CrN in the cubic *Fm*-3*m*[40] and the orthorhombic *Pnma*[31] space group. The refinement parameters are listed in Table 1 and Table 2. The structural phase transition from cubic to orthorhombic can clearly be seen.

Figure 2 also shows a section of the X-ray diffraction patterns recorded between room temperature and 193 K, in steps of 20 K. The reversible phase transition from the cubic (s.g. *Fm*-3*m*) to the orthorhombic crystal system (s.g. *Pnma*) (at 286 K according to literature)[10] can easily be detected. As can be seen in Figure 2 (c) the splitting of the cubic (222) reflection at $2\theta = 34.49°$ indicates that the phase transition occurs between 273 K and 253 K. Below 253 K, the orthorhombic (022), (402) and (122) reflections are visible. In bulk CrN, this phase transition is magnetostructural in nature and marks a reversible change from paramagnetic (high temperature) to antiferromagnetic (low temperature) behavior.

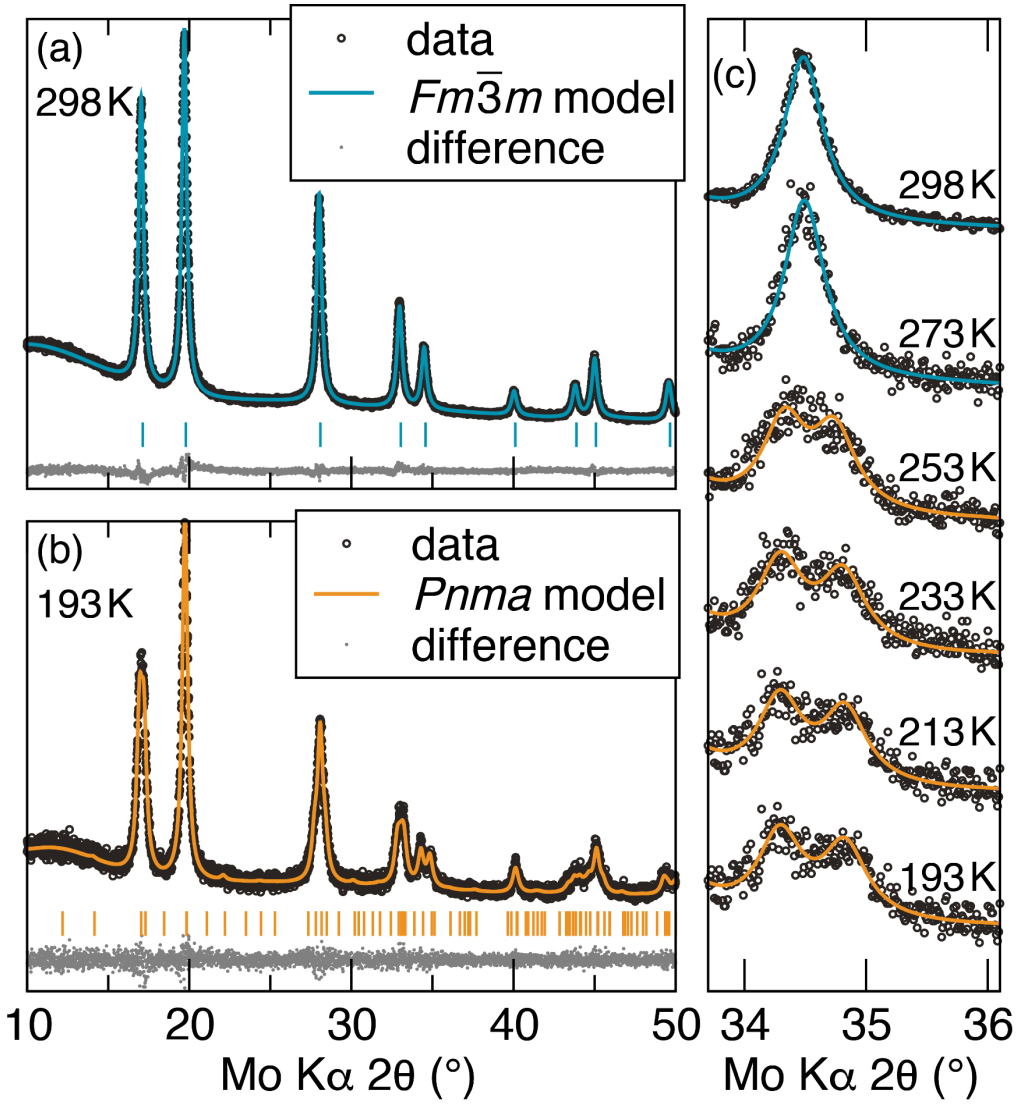

Figure 2: *In-situ* low temperature X-ray powder diffraction data of the annealed (873 K) CrN nanoparticles after Rietveld refinement with the structure of (a) cubic CrN (*Fm*-3*m*)[40] collected at 298 K and (b) orthorhombic CrN (*Pnma*)[31] collected at 193 K. (c) shows the splitting of the cubic (222) peak into the orthorhombic (022), (402) and (122) peaks upon cooling through the structural transition.

Table 1: Rietveld refinement data for the long scan of CrN after annealing at 873 K collected at 298 K.

Temperature / K	298
Space group	*Fm*-3*m*
***a* / Å**	4.14604(8)
***b* / Å**	-
***c* / Å**	-
***V* / Å^3**	71.269(4)
Particle size / nm	13.2 (1)
R_{exp}	2.65
R_{wp}	4.27
GOF	1.61

Table 2: Rietveld refinement data for the short scans of CrN after annealing at 873 K, collected at 298, 273, 268, 263, 258, 253, 233, 213 and 193 K.

T / K	298	273	268	263	258	253	233	213	193
Space group	*Fm*-3*m*	*Fm*-3*m*	*Fm*-3*m*	*Fm*-3*m*	*Pnma*	*Pnma*	*Pnma*	*Pnma*	*Pnma*
***a* / Å**	4.1435 (2)	4.1435(3)	4.1433(3)	4.1428(3)	5.820(2)	5.799(2)	5.787(2)	5.784(2)	5.783(2)
***b* / Å**	-	-	-	-	2.9459(9)	2.9504(6)	2.9566(6)	2.9575(5)	2.9588(5)
***c* / Å**	-	-	-	-	4.141(2)	4.141(2)	4.1341(9)	4.1338(9)	4.1310(8)
***V* / Å^3**	71.13(2)	71.14(2)	71.13(2)	71.10(2)	71.00(4)	70.85(3)	70.73(3)	70.71(3)	70.68(2)
***pseudocubic a* / Å**	-	-	-	-	4.1407(9)	4.1367(6)	4.1369(6)	4.1364(6)	4.1370(5)
***pseudocubic c* / Å**	-	-	-	-	4.141(2)	4.141(2)	4.1341(9)	4.1338(9)	4.1310(8)
***pseudocubic* γ / °**	90	90	90	90	89.29(3)	89.01(2)	88.76(2)	88.71(2)	88.68(2)
R_{exp}	9.92	9.75	9.46	9.48	9.77	10.04	10.14	10.21	10.16
$R_{wp,\ Fm\text{-}3m}$	9.68	9.82	9.47	9.54	10.05	10.08	10.99	11.49	11.37
$R_{wp,\ Pnma}$	9.65	9.80	9.46	9.48	9.77	9.30	9.46	9.56	9.37

The structural transition from *Fm*-3*m* (cubic rocksalt) to *Pnma* (orthorhombic) can be understood as an elongation of the cubic cell along the [110] direction. This results in a monoclinic cell with a unique *c* axis ($a = b \neq c$, $\alpha = \beta = 90°$, $\gamma \neq 90°$). The symmetry of the resulting structure is formally described as *Pnma* by choosing an orthorhombic unit cell, as shown in Figure 3 (a) – (b); however, it is instructive to consider the distorted cubic (pseudocubic) monoclinic unit cell to understand the structural distortion. Upon cooling below the transition temperature, the cubic cell elongates along the [110] direction and the *c* axis deviates from the *a* and *b* axes, which remain equal. Therefore, the transition can be monitored as a deviation of γ from 90° (Figure 3 (d)) and a splitting of the $a = b$ and *c* lattice parameters. The relation of the orthorhombic cell ($a' \neq b' \neq c'$, $\alpha' = \beta' = \gamma' = 90°$) to this pseudocubic monoclinic cell is as follows:

$$\gamma = 2\tan^{-1}\frac{a'}{2b'} \qquad a = \sqrt{1a'/2a^2\ 2\ b'^2} \qquad c = c'$$

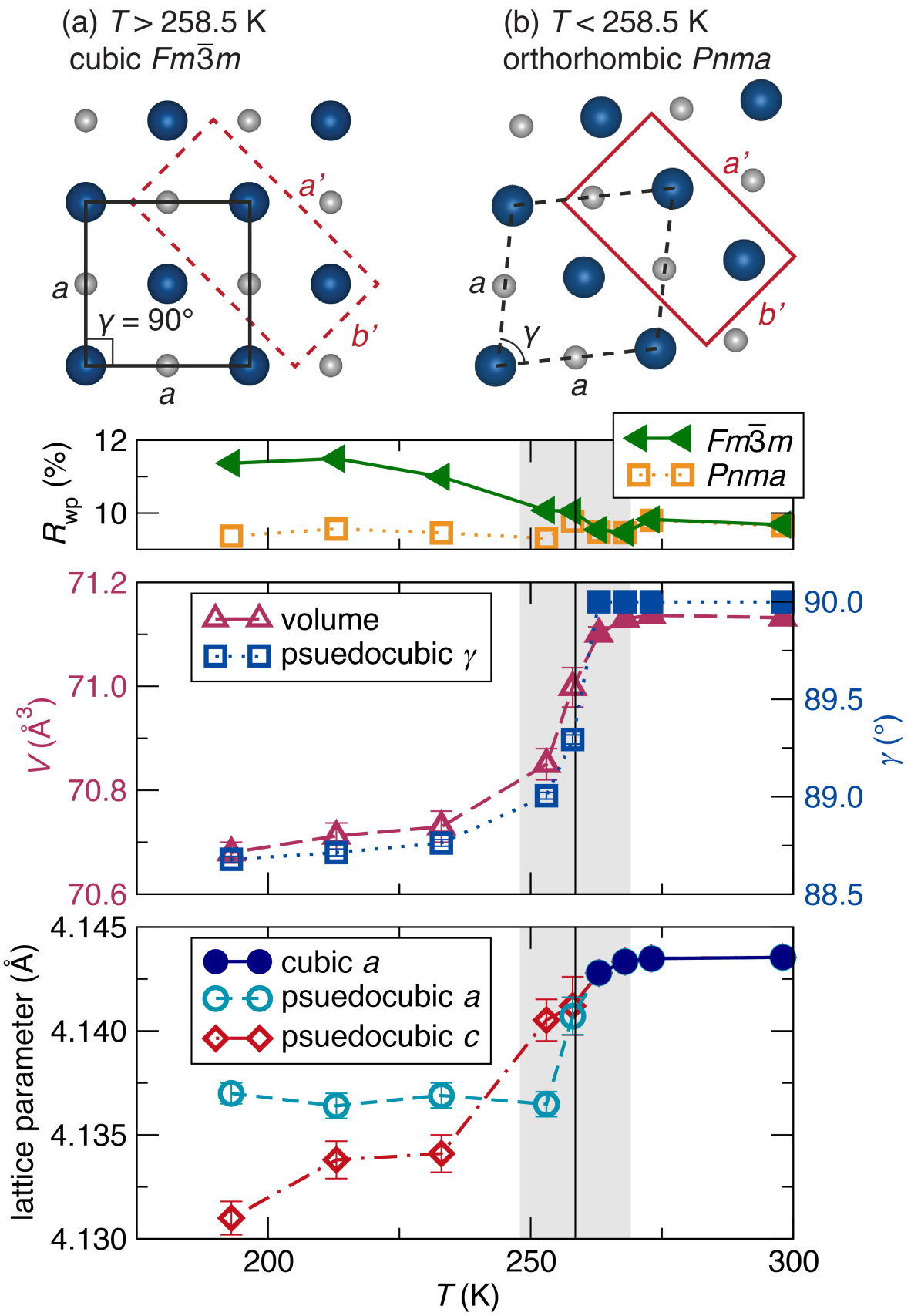

Figure 3: (a)-(b) Drawing of the *ab* plane of CrN in the high temperature cubic structure (a) and the low temperature orthorhombic structure (b). The structural distortion is exaggerated for clarity. The pseudocubic monoclinic cell (black), is used to describe the distorted structure rather than the

orthorhombic cell (red). (c) R_{wp} from refinement of the *in-situ* XRD data in the two space groups. The magnetic transition temperature (258.5 K) is indicated as a solid vertical line. Above this temperature, the *Fm*-3*m* space group fits the data as well as the *Pnma* subgroup. Below the transition temperature, the *Pnma* space group is needed to accommodate the structural distortions that have occurred. (c) The volume of the unit cell and pseudocubic γ both decrease across the structural transition temperature. (d) At the transition temperature, the cubic *a* and *c* lattice parameters split. The *a* parameter is nearly constant below the transition, while the *c* parameter decreases as the temperature decreases. The vertical black line and vertical grey box represent, respectively, the temperature of the center of the magnetic transition (258.5 K) and the approximate transition width (248 K – 269 K).

To investigate whether the structural transition in nanoscale CrN maintains its coupling to a magnetic transition, we performed magnetic and calorimetric measurements on the sample that was annealed at 773 K (Figure 4). Indeed, we observe a clear antiferromagnetic transition in the magnetic data and a corresponding peak in the heat capacity as determined by DSC. The centers of the transitions observed in these two measurements occur at the same temperature (within the error of the thermometry of the two instruments), 258.5 K. This phase transition temperature is consistent with the temperature of the structural phase transition seen in the XRD data. These data suggest that the nanoparticles undergo a single, coupled magnetostructural phase transition as is observed in bulk CrN. Because the SQUID and DSC measurements were taken while sweeping and therefore exhibit some instrumental thermal lag, it is difficult to say whether the transition shows that thermal hysteresis is present, as it is in bulk CrN[41]. However, the peak in heat capacity does suggest that the first-order nature of the transition is maintained in the nanoparticles despite their small size and disorder from their surface.

This magnetostructural transition temperature is about 15 K lower than observed for bulk CrN (273 K – 286 K).[9,30,41] The magnetic transition temperature of nanoparticles is generally lower than for corresponding bulk materials due to the increasing strength of thermal vibrations relative to spin-spin interaction energies[21,42-47]. Interestingly, in the case of CrN, we see the magnetic and structural transition decrease together and remain coupled. In many cases, bulk functional properties such as magnetic and/or structural transitions are observed to be modified or absent in nanoparticles of the same composition.[44,46,48,49] In such a case, it can be difficult to determine whether these differences are due to a size-dependence of the property, or are simply a result of measurement difficulties, off-stoichiometry or impurities.[42,50,51] The present contribution demonstrates that pronounced magnetostructural coupling can be observed in pure nanoparticles. Besides confirming the quality of the nanoparticles produced by the present method, this observation indicates that the magnetostructural effect in CrN does not require long-range periodicity beyond 10 nm.

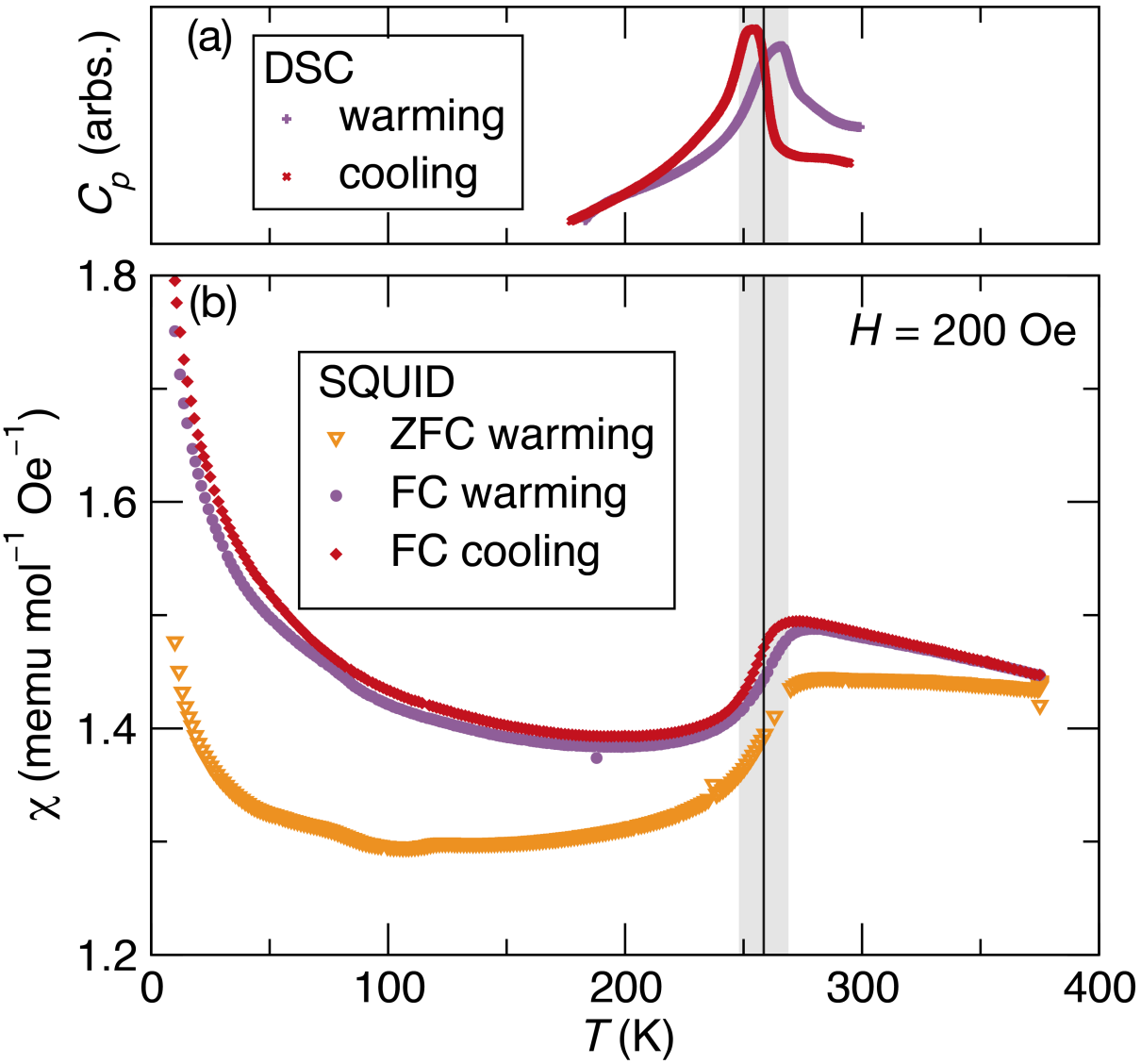

Figure 4: Magnetization as a function of temperature at a fixed field H = 200 Oe (b) and heat capacity from DSC (a) for the CrN nanoparticles. The magnetization *vs*. temperature sweeps were performed first by cooling in zero-field to low temperature and then by measuring upon warming (zero field-cooled warming), and then measuring while cooling back down with the field applied (field-cooled cooling) and then warming once again (field-cooled warming). The vertical black line and vertical grey box represent, respectively, the temperature of the center of the transition (258.5 K) and the transition width (248 K – 269 K), which coincide for both measurement probes.

Conclusion

In conclusion, nearly oxygen- and carbon-free, single-phase CrN nanoparticles (9.8 (± 5.7) nm) can be produced using the method described here. The phase transition from cubic to orthorhombic could be observed at 258.5 K by *in-situ* low-temperature X-ray diffraction, differential scanning calorimetry and SQUID measurements for the first time for nanoscale CrN. Such nanoparticles could possibly be sintered to produce very hard, dense refractory materials.

Supporting Information. Temperature programs used for the annealing of the chromium nitride nanoparticles, particle size distribution of chromium nitride after annealing at 773 K, energy-dispersive X-ray spectroscopy of the chromium nitride nanoparticles after annealing at 773 K, elemental analysis of the chromium nitride nanoparticles after annealing at 773 K, comment on a possible reaction mechanism.

REFERENCES

[1] Dunsmore, D. V.; Patrovsky H. Medical device having a smooth, hardened surface with chromium nitride. U.S. Patent 20050164041 A1, July 28, 2005.

[2] Sartor, J. D.; Robinson, W. E.; Boucher, T. W. Non-stick coated electrosurgical instruments comprising titanium nitride coating, chromium nitride coating, and hexamethyldisiloxane plasma coating, and method for manufacturing the same. U.S. Patent 20170119456 A1, May 4, 2017.

[3] Eklund, P.; Kerdsongpanya, S.; Alling, B. Transition-metal-nitride-based thin films as novel energy harvesting materials. *J. Mater. Chem. C* **2016**, *4*, 3905-3914.

[4] Balogun, M.-S.; Huang, Y.; Qiu, W.; Yang, H.; Ji, H.; Tong, Y. Updates on the development of nanostructured transition metal nitrides for electrochemical energy storage and water splitting. *Mater. Today* **2017**, *20*, 425-451.

[5] Wu, M.; Lin, X.; Wang, Y.; Wang, L.; Guo, W.; Qi, D.; Peng, X.; Hagfeldt, A.; Grätzel, M.; Ma, T. Economical Pt-Free Catalysts for Counter Electrodes of Dye-Sensitized Solar Cells. *J. Am. Chem. Soc.* **2012**, *134*, 3419-3428.

[6] Jankovský, O.; Sedmidubský, D.; Huber, Š.; Šimek, P.; Sofer, Z. Synthesis, magnetic and transport properties of oxygen-free CrN ceramics. *J. Eur. Ceram. Soc.* **2014**, *34*, 4131-4136.

[7] Wang, L.; Jiang, W.; Chen, L.; Yang, M.; Zhu, H. Consolidation of Nano-Sized TiN Powders by Spark Plasma Sintering. *J. Am. Ceram. Soc.* **2006**, *89*, 2364-2366.

[8] Jin, X.; Gao, L.; Sun, J. Preparation of nanostructured $Cr_{1-x}Ti_xN$ ceramics by spark plasma sintering and their properties. *Acta Mater.* **2006**, *54*, 4035-4041.

[9] Filippetti, A.; Pickett, W. E.; Klein, B. M. Competition between Magnetic and Structural Transitions in CrN. *Phys. Rev. B* **1999**, *59*, 7043-7050.

[10] Rivadulla, F.; Banobre-Lopez, M.; Quintela, C. X.; Pineiro, A.; Pardo, V.; Baldomir, D.; Lopez-Quintela, M. A.; Rivas, J.; Ramos, C. A.; Salva, H.; Zhou, J. S.; Goodenough, J. B. Reduction of the bulk modulus at high pressure in CrN. *Nat. Mater.* **2009**, *8*, 947-951.

[11] Alling, B.; Marten, T.; Abrikosov, I. A. Questionable collapse of the bulk modulus in CrN. *Nat. Mater.* **2010**, *9*, 283-284.

[12] Rades, S.; Kraemer, S.; Seshadri, R.; Albert, B. Size and Crystallinity Dependence of Magnetism in Nanoscale Iron Boride, α-FeB. *Chem. Mater.* **2014**, *26*, 1549-1552.

[13] Zhang, Z.; Liu, R.; Qian, Y. Synthesis of nanocrystalline chromium nitride from ammonolysis of chromium chloride. *Mater. Res. Bull.* **2002**, *37*, 1005-1010.

[14] Li, Y.; Gao, L.; Li, J.; Yan, D. Synthesis of Nanocrystalline Chromium Nitride Powders by Direct Nitridation of Chromium Oxide. *J. Am. Ceram. Soc.* **2002**, *85*, 1294-1296.

[15] Schlessinger, G. G. *Inorganic laboratory preparations*; Chemical Publishing Company: New York, 1962.

[16] Cai, P.; Zhu, J.; Yang, Z.; Qian, Y. Synthesis of one-dimensional nanostructure of chromium nitride. *Mater. Chem. Phys.* **2006**, *95*, 1-4.

[17] Tavares, J.; Coulombe, S.; Meunier, J. L. Synthesis of cubic-structured monocrystalline titanium nitride nanoparticles by means of a dual plasma process. *J. Phys. D: Appl. Phys.* **2009**, *42*, 102001.

[18] Feng, W. J.; Li, D.; Li, W. F.; Ma, S.; Li, Y. B.; Xiong, D. K.; Zhang, W. S.; Zhang, Z. D. Structure and Magnetic Properties of Cr(N)-β-Cr_2N Nanoparticles Prepared by Arc-discharge. *J. Alloys Compd.* **2006**, *425*, 4-9.

[19] Yang, X.; Li, C.; Yang, L.; Yan, Y.; Qian, Y. Reduction-Nitridation Synthesis of Titanium Nitride Nanocrystals. *J. Am. Ceram. Soc.* **2003**, *86*, 206-208.

[20] Giordano, C.; Erpen, C.; Yao, W.; Milke, B.; Antonietti, M. Metal Nitride and Metal Carbide Nanoparticles by a Soft Urea Pathway. *Chem. Mat.* **2009**, *21*, 5136-5144.

[21] Zieschang, A.-M.; Bocarsly, J. D.; Dürrschnabel, M.; Molina-Luna, L.; Kleebe, H.-J.; Seshadri, R.; Albert, B. Nanoscale Iron Nitride, ε-Fe_3N: Preparation from Liquid Ammonia and Magnetic Properties. *Chem. Mater.* **2017**, *29*, 621-628.

[22] Gyger, F.; Bockstaller, P.; Gerthsen, D.; Feldmann, C. Ammonia-in-oil-microemulsions and their application. *Angew. Chem. Int. Ed.* **2013**, 52, 12443-12447.

[23] Han, Z.; Zhu, H. M. A Novel Method for the Preparation of Nano-Sized Nickle Powders. *Adv. Mater. Res.* **2012**, *512-515*, 1849-1853.

[24] Yuan, B.; Yang, M.; Zhu, H. Titanium Nitride Nanopowders produced via sodium reduction in liquid ammonia. *J. Mater. Res.* **2009**, *24*, 448-451.

[25] Watt, G. W. Reactions of Inorganic Substances with Solutions of Metals in Liquid Ammonia. *Chem. Rev.* **1950**, *46*, 289-315.

[26] Lagowski, J. J. Liquid Ammonia. *Synth. React. Inorg., Met.-Org., Nano-Met. Chem.* **2007**, *37*, 115-153.

[27] Nicholls, D. *Topics in Inorganic and General Chemistry, Monograph 17: Inorganic Chemistry in Liquid Ammonia*; Elsevier Scientific Publishing Company: Amsterdam, 1979.

[28] Thompson, J. C. *Electrons in Liquid Ammonia*; Oxford University Press: Oxford, 1976.

[29] Schmitz-Dumont, O.; Pilzecker, J.; Piepenbrink, H. F. Über die Amide des dreiwertigen Chroms und Kobalts. *Z. Anorg. Allg. Chem.* **1941**, *248*, 175-207.

[30] Filippetti, A.; Hill, N. A. Magnetic Stress as a Driving Force of Structural Distortions: The Case of CrN. *Phys. Rev. Lett.* **2000**, *85*, 5166-5169.

[31] Corliss, L. M.; Elliot, N.; Hastings, J. M. Antiferromagnetic Structure of CrN. *Phys. Rev.* **1960**, *117*, 929-935.

[32] Alling, B.; Marten, T.; Abrikosov, I. A. Effect of magnetic disorder and strong electron correlations on the thermodynamics of CrN. *Phys. Rev. B* **2010**, *82*, 184430.
[33] Wang, S.; Yu, X.; Zhang, J.; Chen, M.; Zhu, J.; Wang, L.; He, D.; Lin, Z.; Zhang, R.; Leinenweber, K.; Zhao, Y. Experimental invalidation of phase-transition induced elastic softening in CrN. *Phys. Rev. B* **2012**, *86*, 064111.
[34] Bhobe, P. A.; Chainani, A.; Taguchi, M.; Takeuchi, T.; Eguchi, R.; Matsunami, M.; Ishizaka, K.; Takata, Y.; Oura, M.; Senba, Y.; Ohashi, H.; Nishino, Y.; Yabashi, M.; Tamasaku, K.; Ishikawa, T.; Takenaka, K.; Takagi, H.; Shin, S. Evidence for a Correlated Insulator to Antiferromagnetic Metal Transition in CrN. *Phys. Rev. Lett.* **2010**, *104*, 236404.
[35] Liang, Y.; Yuan, X.; Zhang, W. The effect of magnetostructural coupling on mechanical behaviors in CrN. *Solid State Commun.* **2010**, *150*, 2045-2048.
[36] Alam, K.; Disseler, S. M.; Ratcliff, W. D.; Borchers, J. A.; Ponce-Pérez, R.; Cocoletzi, G. H.; Takeuchi, N.; Foley, A.; Richard, A.; Ingram, D. C.; Smith, A. R. Structural and magnetic phase transitions in chromium nitride thin films grown by rf nitrogen plasma molecular beam epitaxy. *Phys. Rev. B* **2017**, *96*, 104433.
[37] Rojas, T.; Ulloa, S. E. Strain fields and electronic structure of antiferromagnetic CrN. *Phys. Rev. B* **2017**, *96*, 125203.
[38] Program TOPAS 4.2, Bruker AXS: Karlsruhe, Germany, **2009**.
[39] Mitchell, D. R. G. DiffTools: Electron diffraction software tools for Digital Micrograph™. *Microsc. Res. Tech.* **2008**, *71*, 588-593.
[40] Blix, R. Röntgenanalyse des Chrom-Stickstoffsystems nebst einer orientierten Konstitutionsuntersuchung des stickstoffhaltigen Ferrochroms. *Z. Phys. Chem. B* **1929**, *3*, 229-239.
[41] Browne, J. D.; Liddell, P. R.; Street, R.; Mills, T. An investigation of the antiferromagnetic transition of CrN. *Phys. Status Solidi A* **1970**, *1*, 715-723.
[42] Mørup, S.; Madsen, D. E.; Frandsen, C.; Bahl, C. R. H.; Hansen, M. F. Experimental and theoretical studies of nanoparticles of antiferromagnetic materials. *J. Phys.: Condens. Matter* **2007**, *19*, 213202.
[43] Lang, X. Y.; Zheng, W. T.; Jiang, Q. Size and interface effects on ferromagnetic and antiferromagnetic transition temperatures. *Phys. Rev. B* **2006**, *73*, 224444.
[44] Kodama, R. H. Magnetic nanoparticles. *J. Magn. Magn. Mater.* **1999**, *200*, 359-372.
[45] Zheng, X. G.; Xu, C. N.; Nishikubo, K.; Nishiyama, K.; Higemoto, W.; Moon, W. J.; Tanaka, E.; Otabe, E. S. Finite-size effect on Néel temperature in antiferromagnetic nanoparticles. *Phys. Rev. B* **2005**, *72*, 014464.
[46] Kodama, R. H.; Makhlouf, S. A.; Berkowtiz, A. E. Finite Size Effects in Antiferromagnetic NiO Nanoparticles. *Phys. Rev. Lett.* **1997**, *79*, 1393-1396.
[47] Ghosh, M.; Biswas, K.; Sundaresan, A.; Rao, C. N. R. MnO and NiO nanoparticles: synthesis and magnetic properties. *J. Mater. Chem.* **2006**, *16*, 106-111.

[48] Senevirathne, K.; Tackett, R.; Kharel, P. R.; Lawes, G.; Somaskandan, K.; Brock, S. L. Discrete, Dispersible MnAs Nanocrystals from Solution Methods: Phase Control on the Nanoscale and Magnetic Consequences. *ACS Nano* **2009**, *3*, 1129-1138.

[49] Tobia, D.; Winkler, E.; Zysler, R. D.; Granada, M.; Troiani, H. E. Size dependence of the magnetic properties of antiferromagnetic Cr_2O_3 nanoparticles. *Phys. Rev. B* **2008**, *78*, 104412.

[50] Tian, P.; Zhang, Y.; Senevirathne, K.; Brock, S. L.; Dixit, A.; Lawes, G.; Billinge, S. J. L. Diverse Structural and Magnetic Properties of Differently Prepared MnAs Nanoparticles. *ACS Nano* **2011**, *5*, 2970-2978.

[51] Madsen, D. E.; Mørup, S.; Hansen, M. F. On the interpretation of magnetization data for antiferromagnetic nanoparticles. *J. Magn. Magn. Mater.* **2006**, *305*, 95-99.

AUTHOR INFORMATION

Corresponding Authors

*[1] Prof. Dr. Barbara Albert, Technische Universität Darmstadt, Eduard-Zintl-Institute of Inorganic and Physical Chemistry, Alarich-Weiss-Str. 12, 64287 Darmstadt, Germany, albert@ac.chemie.tu-darmstadt.de

*[2] Prof. Dr. Ram Seshadri, University of California, Santa Barbara, Department of Chemistry & Biochemistry, Materials Department, and Materials Research Laboratory, University of California, Santa Barbara CA 93106, U.S.A., seshadri@mrl.ucsb.edu

ACKNOWLEDGEMENT

The authors acknowledge financial support from the Hessen State Ministry of Higher Education, Research and the Arts via LOEWE RESPONSE. The transmission electron microscopes used in this work were partially funded by the German Research Foundation (DFG/INST163/2951). The work at UC Santa Barbara was supported by the National Science Foundation through DMR 1710638. J.D.B. is supported by the National Science Foundation Graduate Research Fellowship Program under Grant No. 1650114. The MRL Shared Experimental Facilities are supported by the MRSEC Program of the NSF under Award No. DMR 1720256; a member of the NSF-supported Materials Research Facilities Network (www.mrfn.org). We would like to thank Dr. K. Hofmann for the *in-situ* low-temperature XRD measurements and Dr. Rachel Behrens for help with the DSC measurements.

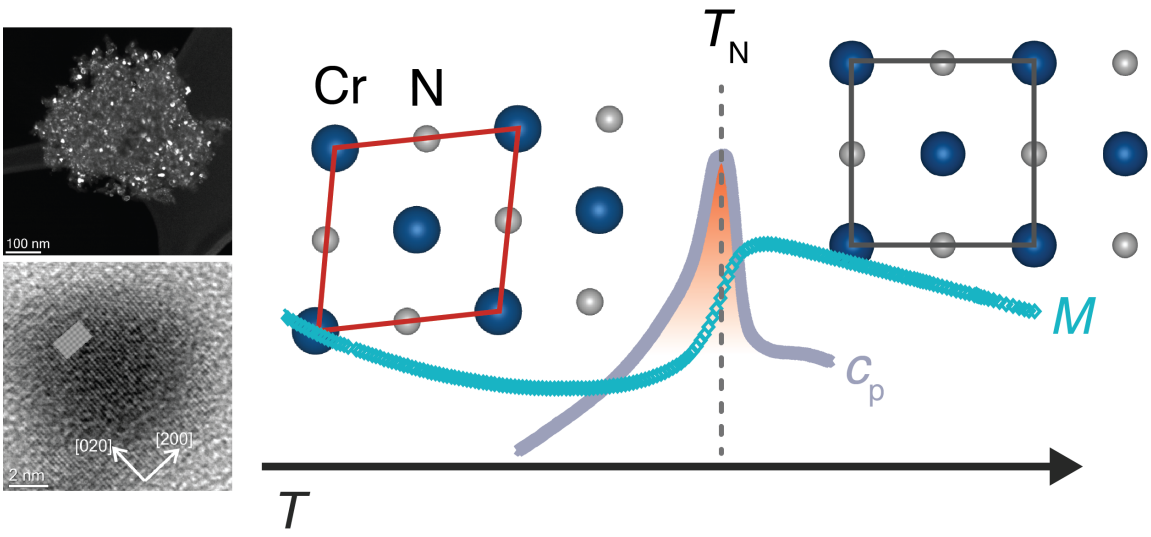
100 nm
2 nm
[020]
[200]
Cr
N
T_N
M
c_p
T

Supporting Information

1. Temperature programs used for the annealing of the chromium nitride nanoparticles

Figure S1 shows the temperature programs that were used for the annealing of the chromium nitride samples in vacuo. The samples were heated slowly to prevent pressure changes during the annealing process.

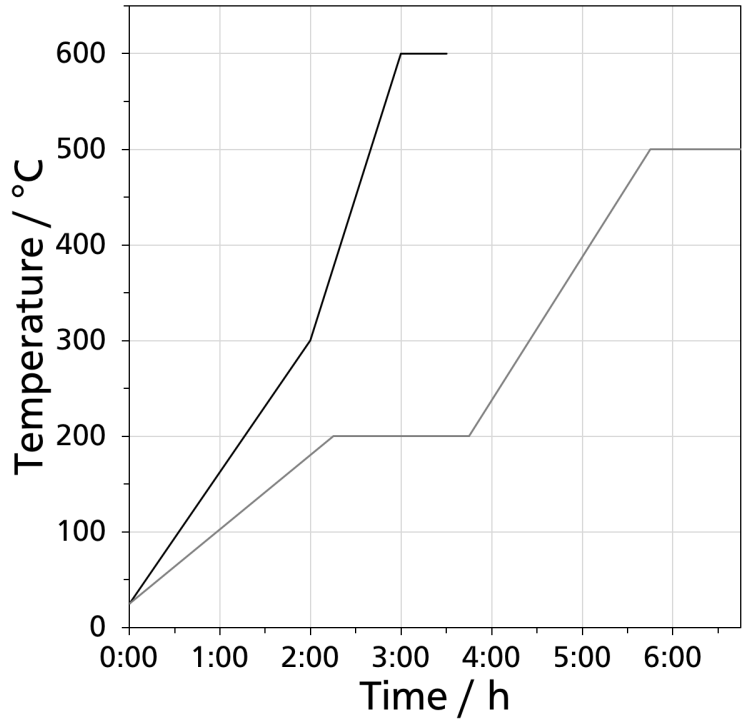

Figure S1: Temperature programs that were used for the annealing of the chromium nitride samples.

2. Particle size distribution of chromium nitride after annealing at 773 K

The particle size distribution of CrN was determined by transmission electron microscopy. Figure S2 shows the particle size distribution for CrN after annealing at 773 K in vacuo.

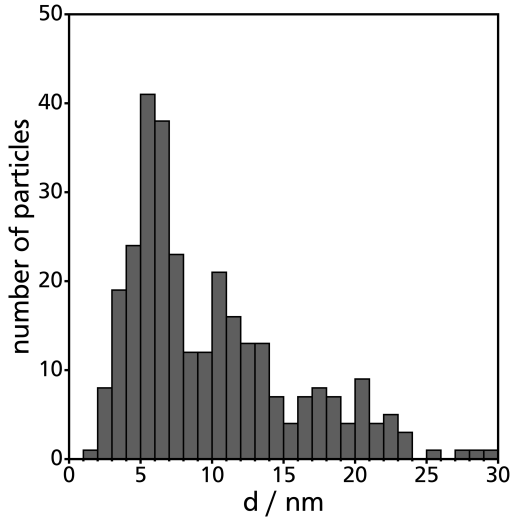

Figure S2: Particle size distributions of CrN after annealing at 773 K as determined by TEM.

3. Energy-dispersive X-ray spectroscopy of the chromium nitride nanoparticles after annealing at 773 K

Table S1: Quantification of EDX spectra of five different particles by the Cliff-Lorimer k-factor method.

	N / at%	Cr / at%
k-factor	3.141	1.120
Spectrum 1	51.73	48.27
Spectrum 2	53.45	46.55
Spectrum 3	52.40	47.60
Spectrum 4	49.73	50.27
Spectrum 5	53.44	46.56
Mean	52.15	47.85
Std. dev.	1.54	1.54

Table 1 shows an EDX quantification of 5 different CrN nanoparticles by the Cliff-Lorimer method. The Cr/N concentration ratio is close to 1:1 as expected. The O-K line lies between two overlapping Cr lines. In detail, it is almost impossible to separate O-K (0.525 keV) from Cr-L_α (0.573 keV) and Cr-L_l (0.500 keV) by using a typical EDX system (energy resolution about 80 eV at O-K). We cannot distinguish between carbon film and carbon that might be included in the CrN nanoparticles.

4. Elemental analysis of the chromium nitride nanoparticles after annealing at 773 K

Elemental analysis was performed to determine the carbon, hydrogen, oxygen, nitrogen and chromium content of the chromium nitride nanoparticles after annealing at 773 K. The results are summarized in Table S2. The analysis was conducted by Mikroanalytisches Labor Pascher, Remagen, Germany. The carbon and hydrogen content were determined using a CH-analyzer (Heraeus/Mannertz/Pascher), the oxygen content using a gas analyzer exhalograph (Balzers) and the nitrogen content according to Dumas using an N-analyzer (Pascher). The chromium content was detected using ICP-AES (iCap 6500, Thermo Instruments).

Table S2: Results of the determination of the carbon, hydrogen, oxygen and chromium content of the chromium nitride nanoparticles by elemental analysis.

Element	Content / wt%
C	0.23 ± 0.046
H	0.055 ± 0.011
O	0.965 ± 0.097
N	21.65 ± 0.65
Cr	76.05 ± 0.77

The composition of the product resulting from the chromium to nitrogen ratio is therefore $CrN_{1.06}$. The oxygen, hydrogen and carbon impurities are most likely caused by residual methanol that is adsorbed on the nanoparticle surface due to the large surface area.

5. Comment on a possible reaction mechanism

The black solid that was obtained after the evaporation of ammonia was analyzed by X-ray diffraction and found to be amorphous. During the reaction, gas evolution was observed. This could be due to the formation of hydrogen or the evaporation of ammonia. Before washing with methanol sodium chloride was identified as the by-product. One possible reaction mechanism is therefore $2\ Cr^{3+} + 6\ Cl^{-} + 2\ NH_3 + 6\ Na \rightarrow 2\ CrN + 6\ NaCl + 3\ H_2$. However, to be sure, further analysis of the amorphous black solid will be necessary.